The Vertical Structure of Linear Coastal-Trapped Disturbances*

R. M. SAMELSON†

Woods Hole Oceanographic Institution, Woods Hole, Massachusetts

(Manuscript received 1 August 1997, in final form 2 March 1998)

ABSTRACT

The vertical structure of coastal-trapped disturbances in several idealized models of a stably stratified lower atmosphere is examined. The vertical structure and phase speeds of the trapped modes depend on the resting stratification and the height of the orographic step. The presence of a stable layer above the boundary layer inversion increases the gravest-mode phase speed and supports the existence of higher vertical modes. Trapped wave solutions for the step orography are obtained for a lower atmosphere with constant buoyancy frequency. The modes are primarily concentrated below the step but penetrate weakly into the stratified region above the step. The phase speed of the gravest trapped mode is greater than the gravest-mode Kelvin wave speed based on the height of the step. Results from a linear two-layer model suggest that the observed vertical structure of isotherms at the leading edge of a 10–11 June 1994 event may arise during a transition from a directly forced, barotropic, alongshore velocity response to a regime influenced by wave propagation, as the coastal-trapped vertical modes excited by the mesoscale pressure gradients begin to disperse at their respective phase speeds. The results suggest also that the observed vertical structure of alongshore velocity, with largest velocities in the stable layer above the boundary layer, may arise from drag at the sea surface.

1. Introduction

Coastal-trapped disturbances of the lower atmosphere have been observed along the coasts of South Africa (Gill 1977; Jury et al. 1990; Reason and Jury 1990), Australia (Holland and Leslie 1986), and western North America (Dorman 1985, 1987; Mass and Albright 1987; Bond et al. 1996; Mass and Bond 1996). The simplest conceptual model of these disturbances consists of a stably stratified layer of fluid that is set in motion by horizontal pressure gradients induced by synoptic and mesoscale evolution above the stable layer. Blocking by coastal orography prevents the establishment of a geostrophic cross-shore flow in the stable layer, and consequently the pressure gradients drive a coastal-trapped flow along the coast.

The theoretical investigation of these phenomena was begun by Gill (1977), who considered forced Kelvin waves in a shallow water model of the stably stratified layer. These investigations have been continued by Nguyen and Gill (1981), Bannon (1981), Hermann et al. (1990), Reason and Steyn (1990, 1992), Rogerson and Samelson (1995), and Samelson and Rogerson (1996). The first two of these included a second active layer above the coastal orography. Motivated by the U.S. west coast climatology of Mass and Bond (1996), the last of these focused on the response of the shallow water model to an isolated pulse of low pressure forcing. Closely related results were obtained previously by Reason and Steyn (1990), who focused on the response to imposed vertical motion that was presumed to result from divergence and convergence of synoptically forced cross-shore motion. The shallow water model has been primarily interpreted as a direct physical model of a well-mixed marine atmospheric boundary layer capped by a sharp inversion, though a more general interpretation as an approximate model for the evolution of the total amount of dense fluid beneath a fixed level may also be appropriate. A high-resolution (30-km grid spacing) primitive equation numerical model was used by Holland and Leslie (1986) to simulate a disturbance observed along the east coast of Australia.

Detailed observations of a coastal-trapped disturbance along the U.S. west coast during 10–11 June 1994 are reported by Ralph et al. (1998). Thompson et al. (1997) compare a mesoscale numerical model simula-

* Woods Hole Oceanographic Institution Contribution Number 9619.

† Current affiliation: College of Oceanic and Atmospheric Sciences, Oregon State University, Corvallis, Oregon.

Corresponding author address: Dr. R. M. Samelson, College of Oceanic and Atmospheric Sciences, Oregon State University, 104 Ocean. Admin. Bldg., Corvallis, OR 97331-5503.
E-mail: rsamelson@oce.orst.edu

tion to these observations. Since the idealized models have all considered only a single active layer beneath the level of the coastal orography, they have provided only limited insight into the vertical structure of the observed and simulated disturbances. Ralph et al. (1998) point out that the June 1994 event contains higher-order vertical structure, with deformation of the thickness of the stable layer that caps the boundary layer, which cannot be explicitly represented within the shallow water models.

In the present work, several idealized models with more realistic stratification are considered in order to examine the effect of the additional stratification on the vertical structure of the coastal-trapped response. The intent is to begin to bridge the gap between existing theory and the complex structure that arises in observations and simulations. The observed and simulated disturbances appear to be strongly forced and damped, but analysis of the free wave modes is useful to guide understanding of the forced response. Free coastal-trapped modes are obtained for two continuously stratified models of the lower atmosphere in sections 2 and 3. In section 4, the coastal-trapped response of a ''two-and-a-half-layer'' model to an isolated pulse of low pressure forcing is examined. This model is the simplest representation of vertical structure that retains analogs of the two gravest trapped modes of the continuously stratified models. Sections 5 and 6 contain discussion and a brief summary of the results.

2. Internal Kelvin waves with overlying stable layer

a. Equations

In shallow water models, the stable stratification of the lower atmosphere is concentrated entirely in the density discontinuity at the interface between the active layer and the overlying atmosphere, resembling a well-mixed marine atmospheric boundary layer capped by a sharp inversion. However, a stable layer, sometimes hundreds of meters thick, is often found immediately above a capping inversion but below the adjacent coastal orography. It is natural to inquire how such a stable layer will modify the properties of the wave modes. Understanding the structure and dynamics of these modes should aid the analysis of the forced response of more complex models, and the atmosphere itself, in the presence of similar vertical stratification.

In this section, the properties of internal Kelvin waves on a rest state consisting of a neutral boundary layer capped by an inversion and a stable layer with finite thickness are briefly considered. For simplicity, compressibility and moisture are neglected, the Boussinesq approximation is made, and the motion is taken to be adiabatic. Under these conditions, the linear equations of motion are

$$u_t - fv = -p_x/\rho_0 \tag{1}$$

$$v_t + fu = -p_y/\rho_0 \tag{2}$$

$$0 = -p_z - g\rho \tag{3}$$

$$u_x + v_y + w_z = 0 \tag{4}$$

$$\rho_t - \frac{\rho_0}{g} N^2 w = 0, \tag{5}$$

where (u, v, w) are the (x, y, z) components of velocity, p is the disturbance pressure, ρ and ρ_0 are the disturbance and reference densities, and f is the Coriolis parameter. The buoyancy frequency of the rest state is N, where $N^2 = -(g/\rho_0)d\rho_s/dz$ and ρ_s is the density of the rest state.

The stable layer is assumed to lie entirely below the level of the coastal orography, so the fluid is taken to be confined to the region $x < 0$ by a rigid vertical wall at $x = 0$. Stable stratification that extends above the orography is considered below, in section 3. The stratification is neutral in the boundary layer ($\rho_s = \rho_0$, $N = 0$ for $0 < z < h$) and above the stable layer ($\rho_s = \rho_2$, $N = 0$ for $z > H$). The stable stratification has two parts, a density jump $\Delta\rho_1 = \rho_1 - \rho_0 \ll \rho_0$ at $z = h$, representing the inversion that caps the marine atmospheric boundary layer, and a stable layer in $h < z < H$ that has constant buoyancy frequency $N = N_2$, with total density change $\Delta\rho_2 = \rho_2 - \rho_1 \ll \rho_0$ over the layer thickness $d = H - h$ (Fig. 1a). The full stratification may be characterized by the two reduced gravities $\gamma_1 = g\Delta\rho_1/\rho_0$ and $\gamma_2 = N_2^2 d = g\Delta\rho_2/\rho_0$. This qualitative structure is often observed over the lower 500–1000 m of the atmosphere along the U.S. west coast in summer, where representative thicknesses of the boundary layer and the stable layer are each several hundred meters, and representative values of the reduced gravities are 0.15–0.3 m s^{-2}.

For N^2, a general function of z, it is convenient to derive an equation for w (Gill 1982). Solutions of the form $w = W(z)\exp[fx/c + il(y - ct)]$ are sought, with $u = 0$ identically. The cross-shore momentum balance is geostrophic, and W satisfies

$$\frac{d^2W}{dz^2} + \frac{N^2}{c^2}W = 0. \tag{6}$$

This equation is solved here by matching constant-N solutions in the three regions $0 < z < h$, $h < z < H$, $z > H$. At $z = h$, the matching conditions are 1) W continuous and 2) $(dW/dz)^- = (dW/dz)^+ + (\gamma_1/c^2)W^+$, where the $-$ and $+$ refer to values just below and just above $z = h$. The second condition may be derived by integrating (6) across a small region of rapidly changing density, in the standard manner. At $z = H$, both W and dW/dz must be continuous. The bottom boundary condition is $W = 0$ at $z = 0$, and the solution $W = \text{const}$ is allowed in $z > H$, where $N = 0$, representing the

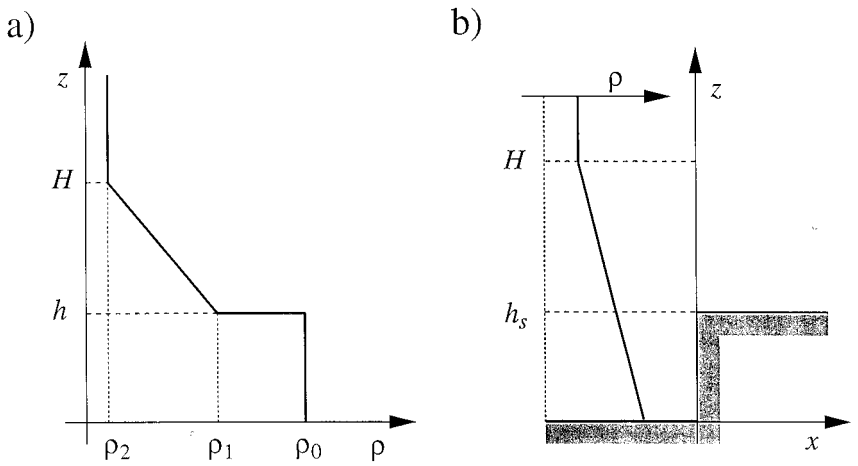

FIG. 1. Stratification and geometry for vertical mode calculations. (a) Neutral boundary layer ($\rho_s = \rho_0$, $z < h$) capped by stable layer with constant stratification ($h < z < H$), as in section 2. (b) Stable layer with constant stratification ($0 < z < H$) overlying orographic step with height h_s at $x = 0$, as in section 3.

limit of weak vertical decay or propagation in a deep upper layer of small N.

The dispersion relation that results from the matching problem may be written

$$\frac{d}{h}\frac{1}{X} - \frac{\gamma_1}{\gamma_2}X = \tan X, \tag{7}$$

where

$$X = \frac{N_2 d}{c} = \frac{(\gamma_2 d)^{1/2}}{c}. \tag{8}$$

b. Results

For all positive boundary layer and stable-layer thicknesses h and d and reduced gravities γ_1 and γ_2, the dispersion relation (7) has one solution for X in the interval $(0, \pi/2)$, corresponding to the first internal Kelvin mode, and one solution for X in each interval $((2k-3)\pi/2, (2k-1)\pi/2)$, $k = 2, 3, \ldots$, corresponding to internal Kelvin mode k, $k \geq 2$. The phase speeds of the first and second mode solutions of (7) are shown in Fig. 2 as a function of d/h for several values of the ratio γ_1/γ_2. Only the first two modes are considered here, since the higher modes have phase speeds that are much smaller than the 5–10 m s^{-1} apparent propagation speeds of observed coastal-trapped disturbances. For example, the second mode phase speed is less than half of the first mode phase speed for $0 < d < 2h$ in Fig. 2.

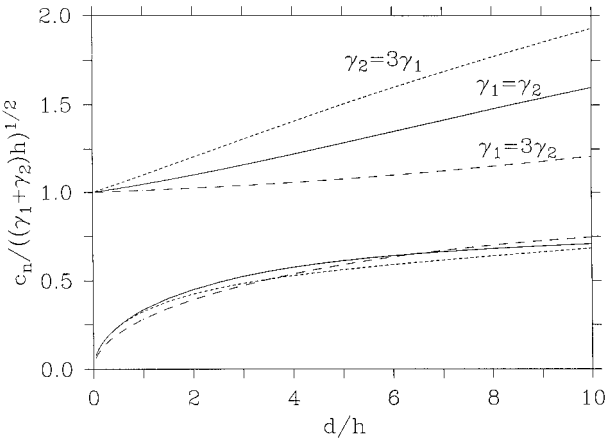

FIG. 2. Normalized Kelvin wave phase speeds c_n/c_0, $c_0 = ((\gamma_1 + \gamma_2)h)^{1/2}$, $n = 1, 2$, vs the ratio d/h of the stable layer and neutral boundary layer thicknesses. Solutions are shown for $\gamma_1/\gamma_2 = \{1/3, 1, 3\}$ (short dashes, solid, long dashes, respectively) for both c_1 and c_2, and the c_1 solutions are labeled accordingly. As $d/h \to 0$, $c_1 \to c_0$, and $c_2 \to 0$.

When the stable-layer thickness d decreases toward zero, the stable layer merges with the inversion, and the gravest mode phase speed c_1 approaches $[(\gamma_1 + \gamma_2)h]^{1/2}$, the shallow water phase speed based on the boundary layer thickness h and the total density difference across the inversion and the stable layer (Fig. 2). In this limit, the stratified layer supporting the higher modes collapses into the inversion, and the phase speeds $c_k \sim d^{1/2}$ all approach zero for $k \geq 2$.

When the stable layer has positive thickness ($d > 0$), $c_1 > [(\gamma_1 + \gamma_2)h]^{1/2}$. Thus, the finite thickness of the stable layer increases the phase speeds for horizontal propagation, relative to the shallow water phase speed based on the boundary layer thickness and the total density difference (Fig. 2). However, a thick stable layer ($d > 2h$) with strong stratification ($\gamma_2 > \gamma_1$) is required to increase the phase speed by more than 10%, relative to the value $[(\gamma_1 + \gamma_2)h]^{1/2}$. Unless γ_2 is small relative to γ_1, the first mode phase speed is always significantly larger than the shallow water phase speed $(\gamma_1 h)^{1/2}$ based on the boundary layer thickness h and the density jump γ_1 across the inversion alone.

When the stable layer is much thicker than the boundary layer ($d \gg h$), the phase speed c_k of the mode-k

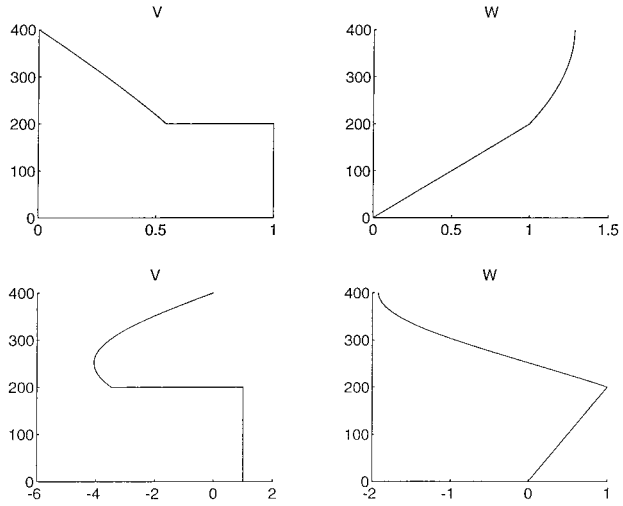

FIG. 3. Vertical structure functions for alongshore velocity (V) and vertical velocity ($W = w/lh$) for modes 1 (upper panels) and 2 (lower panels) for $h = d = 200$ m and $\gamma_1 = \gamma_2$ for the modes in Fig. 2. The units of height (ordinate) are meters.

solution of (7) approaches $c_k^K = (\gamma_2 d)^{1/2}/[\pi(k - 1/2)]$, the mode-$k$ internal Kelvin wave phase speed for a uniformly stratified layer of thickness d.

In the boundary layer ($0 < z < h$), horizontal velocity is vertically uniform, and the amplitude of the vertical velocity increases linearly with height above the surface, for all modes. For the first mode, the horizontal velocity decreases, and the vertical velocity increases, monotonically with height through the inversion layer ($h < z < H$). The higher modes have additional structure in the inversion layer, with the vertical profiles of horizontal and vertical velocity for mode k generally having $k - 1$ zero crossings. Examples of the first and second mode are shown in Fig. 3.

For thick stable layers ($d > 2h$), the second mode phase speed depends less strongly on d/h than the first mode phase speed (Fig. 2). For fixed values of the total density difference ($\gamma_1 + \gamma_2 = \text{const.}$), the second mode phase speed also depends much less on the ratio γ_1/γ_2 than does the first mode phase speed (Fig. 2). Apparently, the presence of an internal zero crossing in vertical velocity allows the second mode to adjust more easily to the surface boundary condition than the first mode, making the second mode less sensitive than the first to the vertical distribution of the stratification.

In summary, stratification consisting of a neutral boundary layer capped by an inversion (density discontinuity), an overlying stable layer, and neutral air aloft, supports an infinite set of internal Kelvin wave modes adjacent to a rigid vertical wall. The first two modes appear to be most relevant in the present context. The stable layer above the inversion increases the phase speed of the gravest mode, relative to phase speeds based on the boundary layer thickness, and allows the infinite set of higher vertical modes to exist.

3. Trapped modes over step orography

a. Equations

In the previous section, the coastal orography was represented by a rigid vertical wall. The horizontal motion was confined vertically to the stably stratified fluid (Fig. 3), suggesting that the wall might be removed at greater altitudes without substantially affecting the internal Kelvin wave modes. Since 300–600-m coastal orography is evidently sufficient to support the observed coastal-trapped disturbances, this would make these results more directly relevant to the interpretation of observed and simulated phenomena.

In this section, this issue is addressed by replacing the vertical wall at $x = 0$ with step orography of height h_s and seeking linear wave modes that are trapped at the step. For simplicity, the neutral boundary layer is removed, and the stably stratified lower atmosphere is represented by a layer of constant buoyancy frequency N that extends from the surface to the constant height $z = H > h_s$ (Fig. 1b). On the low side of the step, $x < 0$, the surface is at $z = 0$. On the high side, $x > 0$, the surface is at $z = h_s > 0$, and the thickness of the stable layer is $d_s = H - h_s < H$. Above the stable layer, $z > H$, the stability is again taken to be neutral ($N = 0$), which prevents vertical propagation and traps the modes near the surface. The equations of motion are again (1)–(5). As in section 2, the structure and dynamics of the wave modes are examined here, in order to aid the analysis of the forced response of more complex models, and the atmosphere itself, in the presence of similar vertical stratification and orography.

Modes are sought that are sinusoidal in time and along the step, so the pressure may be written $p = \rho_0 fLP(x, z)\exp[il(y - ct)]$, where $L = NH/f$ is a deformation radius and the constant factors are inserted for convenience. Then P satisfies

$$P_{\xi\xi} + P_{\zeta\zeta} - \lambda^2 P = 0, \tag{9}$$

where $\xi = x/L'$, $\zeta = z/H$, and $\lambda = lL'$. Here $L' = \delta L$, where $\delta = (1 - l^2c^2/f^2)^{-1/2} = (1 - \lambda^2 c'^2)^{-1/2}$ and $c' = c/fL'$. The boundary conditions are

$$P \to 0 \quad \text{as } |\xi| \to \infty \tag{10}$$

$$P_\zeta = 0 \quad \text{at} \begin{cases} \zeta = 0, & \xi < 0 \\ \zeta = h & \xi > 0 \end{cases} \tag{11}$$

$$P = 0 \quad \text{at } \zeta = 1 \tag{12}$$

$$P^- = P^+ \quad \text{at } \xi = 0,\ h < \zeta < 1 \tag{13}$$

$$c'P_\xi^- - P^- = \begin{cases} c'P_\xi^+ - P^+ & \text{at } \xi = 0,\ h < \zeta < 1 \\ 0 & \text{at } \xi = 0,\ 0 < \zeta < h, \end{cases} \tag{14}$$

where $P^- = P(\xi < 0)$, $P^+ = P(\xi > 0)$, and $h = h_s/H$. Except for the boundary condition (12) at the top of the stable layer, this is identical to the oceanographic problem studied by Chapman (1982), and is solved here as described in appendix A.

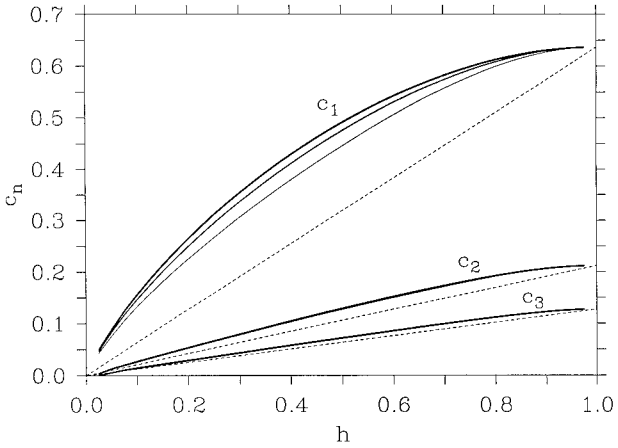

FIG. 4. Dimensionless phase speeds for trapped modes 1, 2, and 3 at step orography of dimensionless height $h = h_s/H$ in a stable layer of thickness H. For each mode, the phase speeds are shown for $\lambda = 0, 1, 2$ (thick, intermediate, and thin lines, respectively). The phase speeds of the corresponding Kelvin modes for a stable layer of thickness h adjacent to a vertical wall are also shown (dashed lines).

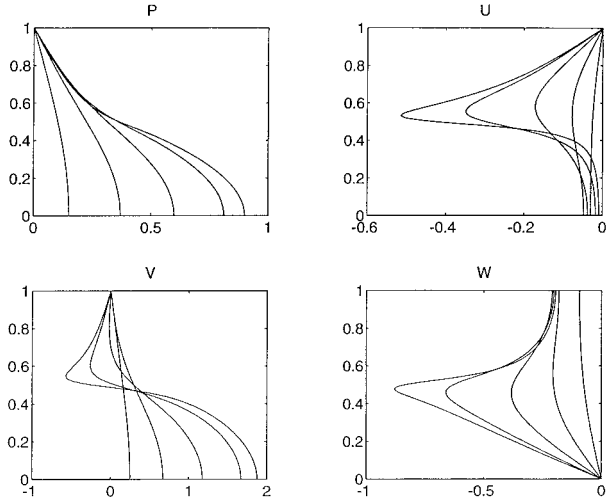

FIG. 5. P, U, V, W for the first mode in Fig. 4, with $h = 0.5$ and $\lambda = 1$. Vertical profiles with z as ordinate are shown at $x/L = \{-1, -0.5, -0.25, -0.1, -0.05\}$. For each set of profiles, maximum amplitudes increase monotonically toward the step. The modes have been scaled so that $P = 1$ at the base of the step ($x = z = 0$).

If the structure functions U, V, W, Z, for horizontal and vertical velocity and vertical displacement of density surfaces, are defined by

$$(u, v, w, \rho) = \left(iU, V, i\frac{H}{L}W, -\frac{H}{fL}\frac{d\rho_s}{dz}Z\right)\exp[il(y - ct)], \quad (15)$$

then

$$U = \lambda\delta(c'P_\xi - P) \quad (16)$$

$$V = \delta(P_\xi - \lambda^2 c'P) \quad (17)$$

$$W = \lambda c'P_\zeta \quad (18)$$

$$Z = -P_\zeta. \quad (19)$$

Thus u and w will generally be out of phase with P, v, and ρ, and the single function P_ζ will describe the structure of both w and ρ.

The dimensionless eigenvalue problem (9)–(14) or (A6) contains two parameters, the step height $h = h_s/H$, where $0 < h < 1$, and the scaled along-step wavenumber λ. For a given dimensionless wavenumber λ, the parameter δ may be computed after the eigenvalue c' has been found. The frequency dependence may then be removed by defining the dimensionless wavenumber $l_* = lL = \lambda/\delta$ and phase speed $c_* = c/(fL) = \delta c'$.

b. Results

The eigenvalue problem (9)–(14) has solutions corresponding to modes that are trapped near the step orography. Since the trapped modes can be expected to resemble internal Kelvin waves in a stable layer of total depth equal to the height of the step h, which have dimensionless phase speeds $c_k^K = h^{1/2}/((k - 1/2)\pi)$, the phase speeds c_k of the trapped modes should approach the phase speeds c_k^K as h approaches one, and the c_k should approach zero as h approaches zero, where $c_k = \delta c_k'$ is the value of c_* for mode k. The numerical solutions verify this expectation (Fig. 4). The trapped modes are nondispersive in both limits.

For intermediate h, that is, when the stable stratification extends appreciably above the step, the trapped mode phase speeds are always greater than the corresponding Kelvin wave phase speeds c_k^K based on the step height (and the fixed buoyancy frequency, the dependence on which has been removed by the nondimensionalization). This enhancement of the trapped mode phase speed by the stable layer above the step is particularly evident for the first mode, for which $c_1 \approx 1.5c_1^K$ at $h = 0.5$. The first mode is weakly dispersive for $0.1 < h < 0.9$, but the higher modes are essentially nondispersive for all h (Fig. 4). The first mode phase speed is several times larger than the second mode phase speed for all h. As $h \to 1$, the ratio c_1/c_2 approaches the corresponding Kelvin wave ratio $c_1^K/c_2^K = 3$. For $h = 0.5$, $c_1/c_2 \approx 4$.

The solutions for $h = 0.5$ and $\lambda = 1$ illustrate the typical structure of modes with $0 < h < 1$, for which the stable layer extends above the step (Figs. 5, 6). The first-mode pressure, along-step velocity v, and vertical velocity and displacement are primarily, but not entirely, confined beneath the step. In contrast, the velocity u normal to the step is large only above $h > 0.5$, where it attains values near $x = 0$ that are of the same order of magnitude as the largest along-step velocities. Thus, the trapped mode resembles an internal Kelvin wave below the step, where cross-step flow is blocked, but has substantial cross-step motion above the step, where cross-step flow is not blocked. Associated with this

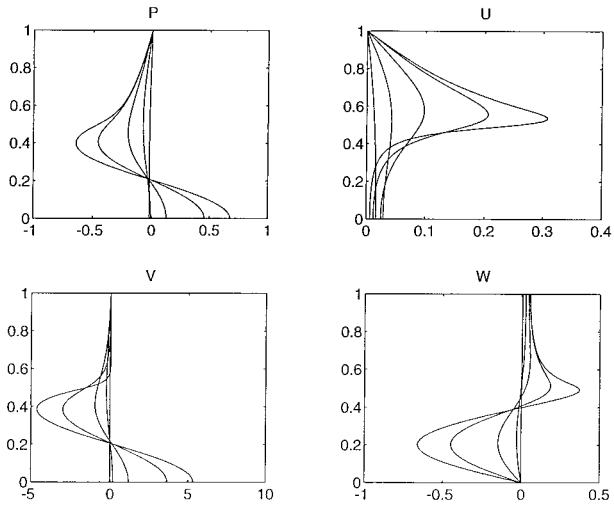

FIG. 6. As in Fig. 5 but for the second mode in Fig. 4.

cross-step motion is a reversal in the first-mode along-step velocity near $x = 0$ and $z = h$. Beneath the step ($z < h$), the disturbance pressure, along-step velocity, and vertical displacement are all in phase, as for an internal Kelvin wave. The pressure and along-step velocity are largest at the surface, while the vertical velocity and vertical displacement are largest at the step height. The pressure and horizontal velocities vanish above the stratified layer. The vertical velocity and displacement are nonzero but relatively small at the top of the stratified layer.

The higher modes have a structure above the step that is similar to the first mode but resembles the corresponding higher internal Kelvin modes below the step, with internal zero crossings (Fig. 6). Their phase speeds are slow (Fig. 4) and their offshore decay scales are small (Fig. 6), relative to the first mode.

In summary, trapped modes exist along the step even when the fluid immediately above the step is stratified. These modes generally behave like internal Kelvin waves in a stratified layer of depth equal to the step height h. However, they are weakly dispersive, their phase speeds may be as much as 50% greater than the corresponding internal Kelvin wave phase speeds, and their motion penetrates into the stratified layer above the step, where substantial cross-step motion occurs near the corner of the step.

Nguyen and Gill (1981) and Bannon (1981) both considered two-layer models of coastal-trapped disturbances in which the upper interface lay above the orographic step height. The two corresponding two-layer modes are roughly analogous to the first two modes of the present problem when $0 < h < 1$. The matching conditions at the step differ in the two cases, however, as normal transport in the upper layer is continuous in the two-layer model, whereas normal velocity is continuous at each point above the step in the present problem. The two-layer model cannot reproduce the detailed vertical structure of the continuously stratified modes, but it does correctly predict that cross-step motion occurs above the step.

4. Forced two-layer reduced-gravity model

a. Motivation

In the preceding sections, two simple models of orographically trapped wave modes in a continuously stratified fluid were examined. The vertical scale of these modes was set by the vertical scale of the stratification or the orography, whichever was smaller. The modes with uniform stratification resembled reduced-gravity internal Kelvin waves. The presence of a neutral surface boundary layer did not cause essential changes in the qualitative features of the modes, though some aspects of the modal structure and propagation characteristics were affected.

Observed coastal-trapped disturbances are a forced-damped response of the orographically blocked lower atmosphere to synoptic and mesoscale evolution. In this section, the linear coastal-trapped response of a simple model of a stably stratified lower atmosphere to pressure forcing is considered. The object is to understand how the forced response is altered from the shallow water model (e.g., Samelson and Rogerson 1996) when the stratification of the blocked fluid is not confined to a density jump across the inversion.

For simplicity, a two-layer reduced-gravity model is used, in which the stratification in the stable layer above the neutral boundary layer is represented by the density difference across the interface between a second homogeneous fluid layer that overlies the neutral boundary layer, and a third, passive layer above. This model is a coarse representation of the vertical structure, relative to the continuously stratified models considered above, but is the simplest context in which the baroclinic structure of the trapped response can be investigated.

The two vertical modes that arise in the two-layer reduced-gravity model are qualitatively similar to the first and second modes in the two continuously stratified models considered in the preceding sections, for which the first modes had monotonic vertical profiles of horizontal and vertical velocity, whereas the second modes had single zero crossings in both profiles. Thus, the results should extend with some generality to models with more detailed representations of the stratification. In contrast to the models considered by Nguyen and Gill (1981) and Bannon (1981), both interfaces are located beneath the height of the coastal orography, which is represented by a vertical wall, so flow in both active layers is blocked. In the following, attention is first restricted to the inviscid coastal-trapped response, as represented by a pair of linear first-order wave equations for the forced Kelvin modes. The response is also computed for the full linear model, with and without surface friction.

b. Equations

In isentropic coordinates, the equations for momentum and mass conservation in a dry, compressible atmosphere may be written

$$u_t + uu_x + vu_y + w_* u_\theta - fv = -M_x + F, \quad (20)$$

$$v_t + uv_x + vv_y + w_* v_\theta + fu = -M_y + G, \quad (21)$$

$$\psi_t + (u\psi)_x + (v\psi)_y + (w_*\psi)_\theta = 0, \quad (22)$$

where (u, v) are the (x, y) components of velocity, $\psi = p_\theta$, $M(x, y, \theta) = g\chi + \theta\Pi$, $z = \chi(x, y, \theta)$ is the height of the isentropic surface with potential temperature θ, p is pressure, and $\Pi(p) = c_p(p/p_s)^\kappa$ is the Exner function, with c_p the specific heat at constant pressure, p_s a reference pressure, $\kappa = R/c_p$, and R the gas constant for dry air. The functions F and G are frictional dissipation terms, and $w_* = \dot{\theta}$ represents diabatic forcing. The hydrostatic relation takes the form $M_\theta = \Pi$. Numerical solutions of these equations using a scheme based on that of Reisner and Smolarkiewicz (1994) are presented below and compared with forced linear Kelvin wave solutions that are discussed first.

As in section 2, the vertical wall is placed at $x = 0$, and the domain is $x < 0$. Forced linear Kelvin wave solutions are obtained as follows. Equations (20)–(22) are linearized around a step profile in potential temperature, $\theta = \theta_1$ for $0 < z < z_1$, $\theta = \theta_2$ for $z_1 < z < z_2$, and $\theta = \theta_3$ for $z > z_2$, and they are forced by an imposed pressure distribution $p_a(y, t)$ at the fixed height $z = H_a > z_2$. The semigeostrophic approximation is also made ($u_t \ll fv$), and the frictional terms are neglected ($F = G = 0$). The resulting forced Kelvin wave solutions may be written

$$\psi_1 = \psi^+ e^{fx/c_+} + \psi^- e^{fx/c_-}, \quad (23)$$

$$\psi_2 = \psi_2^+ e^{fx/c_+} + \psi_2^- e^{fx/c_-}, \quad (24)$$

where $c_\pm$ and $\psi^\pm$ are the first and second internal Kelvin wave mode phase speeds and amplitudes, respectively, and $\psi^\pm$ satisfy the forced first-order wave equations

$$\psi_t^+ + c_+\psi_y^+ = \left(\frac{1 - d_-}{d_+ - d_-}\right)\frac{\Psi_1}{c_+}F_{ay}, \quad (25)$$

$$\psi_t^- + c_-\psi_y^+ = \left(\frac{d_+ - 1}{d_+ - d_-}\right)\frac{\Psi_1}{c_-}F_{ay}. \quad (26)$$

For the first mode ψ^+, the interface displacements are of the same sign. The upper interface displacement is larger than the lower interface displacement, whereas the lower-layer horizontal velocity is larger than the upper-layer horizontal velocity, consistent with the structure of the continuously stratified first modes considered above. For the second mode ψ^-, the interface displacements are of opposing signs, as are the upper- and lower-layer horizontal velocities, consistent with the structure of the continuously stratified second modes considered above. The lower-layer amplitudes $\psi_2^\pm$, the constants Ψ_1, $c_\pm$, and $d_\pm$, and the forcing term F_{ay} are defined in appendix B.

The parameters used below for the rest or initial-state potential temperature profile are $z_1 = 200$ m, $z_2 = 400$ m, $\theta_1 = 290$ K, $\theta_2 = 300$ K, and $\theta_3 = 310$ K. For these parameters, the phase speeds are $c_+ = 13.4$ m s^{-1} and $c_- = 5.0$ m s^{-1}. For the first mode (c_+), the interface displacements Z_1 and Z_2 are of the same sign (but are not equal), whereas for the second mode (c_-), they are of opposing signs. The numerical solutions of the full equations (20)–(22) are obtained in the same configuration, with two active θ levels and pressure imposed at a fixed level in a passive, third, upper layer (making it a ''two-and-a-half-layer'' model). The numerical discretization of the continuous equations is consistent with the interpretation as a layer model. The imposed pressure at $z = 1500$ m consists of a constant (equal to 850 mb) plus a translating Gaussian pulse with amplitude P_F and width 500 km. Initially, the pulse propagates westward toward and into the domain from the east at 5.75 m s^{-1}. Its center reaches the eastern boundary of the domain at $t = 10^5$ s, and it then reverses direction, propagating eastward and out of the domain at 5.75 m s^{-1}. The numerical integrations cover approximately 2.3 days, from $t = 0$ to $t = 2 \times 10^5$ s. The numerical solutions were obtained in a periodic channel geometry, on a 51×251 grid, with 10-km grid spacing across the 500-km width and 20-km grid spacing along the 5000-km length of the channel. The time step was 100 s.

c. Results

The evolution of the linear inviscid model response to the imposed forcing may be divided into three phases: generation, transition, and dispersion. These phases may be illustrated with approximate representations of the coastal-trapped response that were obtained by solving the first-order wave equations (25) and (26) with the parameters given above, forcing amplitude $P_F = -1$ mb, and no friction (Figs. 7 and 8). The phases are not fully distinct but are a useful guide to understanding the overall evolution of the response.

During the generation phase, the amplitude of the disturbance grows locally in direct response to the imposed forcing. This phase is essentially complete by $t = 10^5$ s, when the forcing has reached its maximum, and the disturbance passes into the transition phase, where propagation effects begin to influence the response. At $t = 10^5$ s, the velocity response is approximately equal in both layers, and southerlies extend 200 km north of the central latitude $y = 0$ of the pressure pulse (Fig. 8). The barotropic (depth independent) structure of the alongshore winds is a direct response to the depth independence of the forcing F_{ay}. Although the pressure forcing F_{ay} is the same in each layer, both vertical modes are directly forced (Fig. 7), because a barotropic vertical mode ($\psi_1 = \psi_2$) does not exist. The

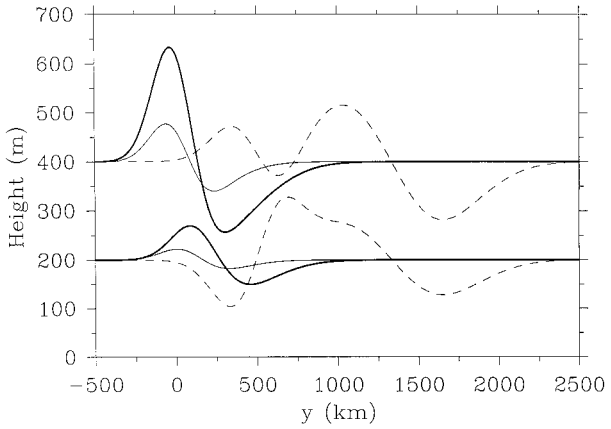

FIG. 7. Solutions of the two-layer forced linear Kelvin wave model. Interface heights at $x = 0$ are shown vs y for $t = 0.75 \times 10^5$ s (thin line), $t = 10^5$ s (thick line), and $t = 2 \times 10^5$ s (dashed line). The pressure forcing amplitude is $P_F = -1$ mb.

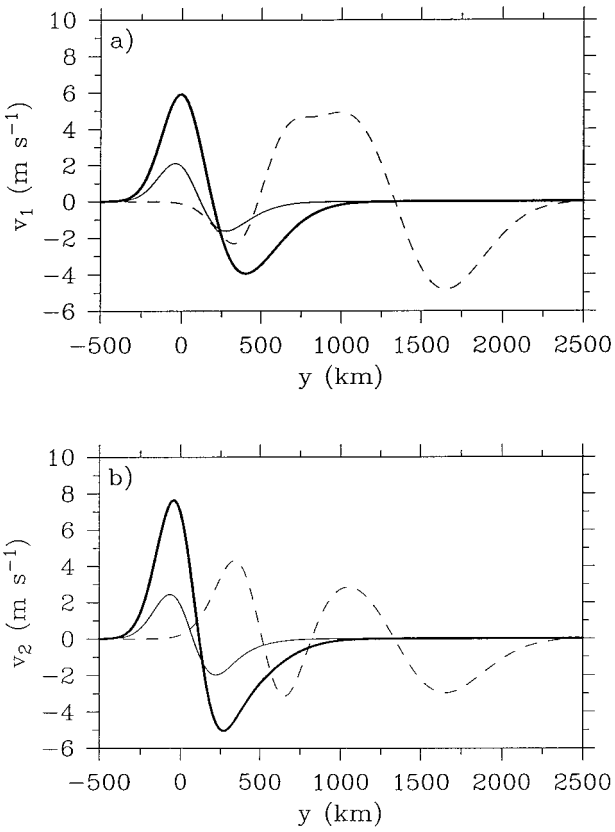

FIG. 8. As in Fig. 7 but for northward velocity in (a) layer 1 and (b) layer 2.

continuously stratified models also lack a barotropic mode (Figs. 3, 5). The geostrophic relations (B1) and (B2) require that $\psi_{1x} \approx 0$ if $v_1 \approx v_2$, and consequently the lower interface displacement is initially much smaller than the upper interface displacement (Fig. 7). Since $\psi_{1x} \approx 0$ only if $\psi^+/c_+ + \psi^-/c_- \approx 0$, both modes are excited initially, but with opposite sign.

In the transition phase, which begins roughly at $t = 10^5$ s, the pressure gradients associated with deformations of the layer interfaces become comparable to the imposed pressure gradient forcing, and wave propagation effects begin to alter the response. It is followed by the dispersion phase, in which wave propagation effects dominate, the excited modes separate because of differences in their phase speeds, and local forcing is negligible. The timescales for propagation of the disturbance out of the forcing region and for dispersive separation of the excited modes may be estimated from the horizontal scale of the forcing region and the phase speeds of the modes. The propagation timescales for the first and second modes are 500 km/13.4 m s^{-1} $\approx$ 0.4 days and 500 km/5.0 m s^{-1} $\approx$ 1.1 days, respectively, whereas the separation timescale is 500 km/(13.4–5.0) m s^{-1} $\approx$ 0.7 days. These should be measured with respect to, say, $t \approx 10^5$ s, when the forcing is maximum. Thus, by $t = 1.5 \times 10^5$ s, the 8 m s^{-1} difference in first- and second-mode phase speeds has already begun to cause separation of the modes. The leading part of the disturbance has a first-mode structure, with depression of both interfaces and northerly winds in both layers, whereas the trailing part has a second-mode structure, with depression of the lower interface, elevation of the upper interface, and flow primarily confined to the upper layer. By $t = 2 \times 10^5$ s, the modal structures are clearly identifiable and overlap only near $700 < y < 1000$ km (Figs. 7, 8).

The first-mode disturbance is qualitatively similar to the disturbance modeled by previous single-layer (shallow water) models of coastal-trapped disturbances (e.g., Samelson and Rogerson 1996), but propagates faster because of the greater stability and greater depth of the stable layer and the absence of an opposing mean flow. By $t = 2 \times 10^5$ s, the southerly transition associated with this first-mode disturbance has propagated 1500 km from the central latitude of the pressure pulse. The slow-moving second-mode disturbance and the complex vertical structure of the initial response have no analogs in the single-layer models. Note that the linear two-layer calculation suggests that nonlinear effects will be important even for pressure forcing of order 1 mb, since the interface deformations are comparable to the layer thicknesses. The slow-moving higher vertical modes should be more susceptible to nonlinear effects than the gravest mode.

Linear solutions of the full two-layer equations (not shown) are similar to the wave-equation solutions. These were obtained by forcing the numerical model with a small-amplitude pulse ($P_F = -0.1$ mb) and then rescaling the response. Despite the qualitative similarity, the amplitude of the propagating response is less than half that obtained from the wave equations. This difference is due primarily to the finite (500-km width) zonal scale of the forcing pulse in the numerical model. If the the pulse is replaced by a time-dependent, zonally

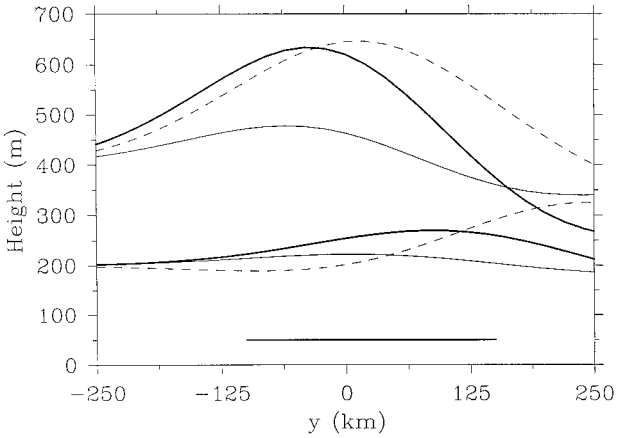

FIG. 9. Solutions of the two-layer forced linear Kelvin wave model. Interface heights at $x = 0$ are shown for -250 km $< y <$ 250 km for $t = 0.75 \times 10^5$ s (thin line), $t = 10^5$ s (thick line), and $t = 1.25 \times 10^5$ s (dashed line). The pressure forcing amplitude is $P_F = -1$ mb. The short horizontal line indicates the 250-km segment to be compared with the aircraft transects of Ralph et al. (1998).

uniform forcing with Gaussian meridional structure, the linear response of the numerical model is close to the approximate result obtained from the wave equations. Some additional linear solutions of the numerical model were obtained with frictional damping. These damped solutions are discussed below.

5. Discussion

The above analysis has shown that the barotropic forcing of the stable layer by imposed pressure gradients generates a baroclinic coastal-trapped response in the stable layer. The barotropic forcing initially generates a barotropic response in alongshore winds throughout the stable layer. Since the alongshore flow must remain approximately geostrophic near the coastal barrier, the upper part of the stable layer deforms to provide a depth-independent geostrophic pressure gradient, whereas the isotherms in the lower part of the stable layer are initially undisturbed, consistent with the barotropic structure of the initial alongshore wind response. Consequently, both vertical modes are excited in the two-layer model, and generally all vertical modes will be excited in a continuously stratified model, though high vertical modes will be only weakly excited. Deformations of the lower isotherms and a baroclinic velocity structure then develop in the linear model as the excited modes disperse at their respective phase speeds, and a transition occurs to a regime dominated by free-wave propagation.

The transition phase, from directly forced local response toward a regime dominated by wave propagation, occurs as the forcing reaches its maximum and then decays, primarily between $t = 10^5$ s and $t = 1.5 \times 10^5$ s, and in the region -250 km $< y <$ 500 km. The layer interfaces and alongshore velocities at $x = 0$ during this transition include both directly forced and

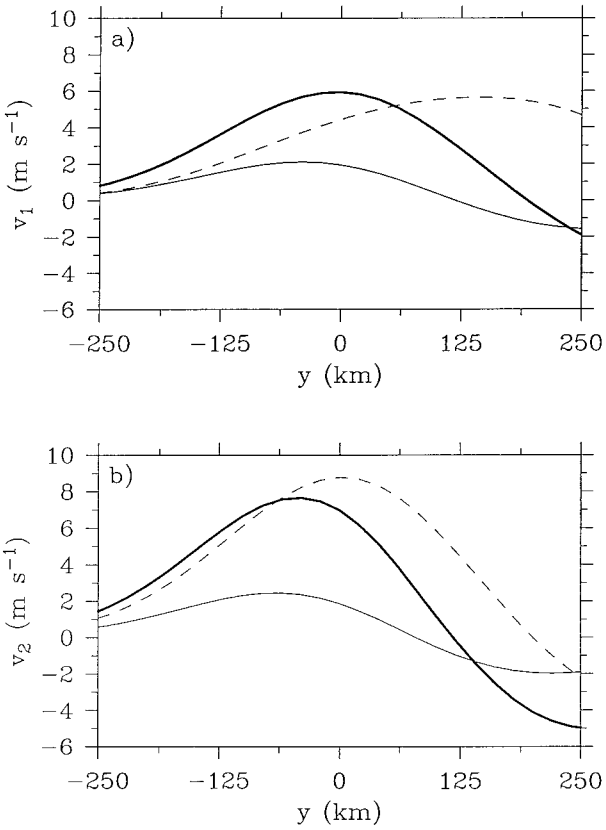

FIG. 10. As in Fig. 9 but for northward velocity in (a) layer 1 and (b) layer 2.

wavelike components, as the directly forced flow creates internal pressure gradients by deforming the layer interfaces, which in turn accelerate the flow. At $t = 0.75 \times 10^5$ s, the alongshore velocities are nearly barotropic, and the upper interface displacement is an order of magnitude greater than the lower interface displacement (Figs. 9 and 10). At $t = 10^5$ s, baroclinic structure in the velocity field has begun to develop, with differences of 2–5 m s^{-1} between layers, and the lower interface displacement has reached 100 m. At $t = 1.25 \times 10^5$ s, there are velocity differences of 5–10 m s^{-1} between layers, and the lower interface displacement is comparable to the upper interface displacement for 150 km $< y <$ 500 km. The maximum lower-layer velocity has shifted 200 km north of the maximum upper-layer velocity by this time. At later times, the imposed pressure forcing is small, and the evolution of the flow is controlled by the dispersion of the modes (Figs. 7 and 8).

The Bond et al. (1996) and Mass and Bond (1996) coastal-trapped disturbance climatology has been briefly compared by Samelson and Rogerson (1996) to the life cycle of an idealized coastal-trapped disturbance in a one-layer reduced-gravity (shallow water) model, and some qualitative similarities were found. Because of the limitations of existing observations, the climatology did not resolve vertical structure between 850 mb and the

surface, which is the focus of the present study. Vertical structure at these levels was resolved by aircraft and profiler observations of a coastal-trapped event that occurred during 10–11 June 1994 along the U.S. west coast (Ralph et al. 1998), and these may be compared with the present model.

The synoptic and mesoscale pressure evolution during the June 1994 event included warm offshore advection above the marine boundary layer that altered the pressure distribution in the boundary layer and the overlying stable layer, and also modified the overlying stable layer directly (Ralph et al. 1998). The linear model is forced solely by imposed changes in the pressure field above the stable layer, and consequently only part of the effect of warm advection on the overlying stable layer is captured. Nonetheless, some of the baroclinic structure observed during that event appears qualitatively similar to the linear two-layer solutions during an early stage of the model response. This structure is discussed below. In contrast, analogs of the large-amplitude disturbances that extend 1000–2000 km northward during the final phase of the inviscid model response do not appear to exist in the observations. There are many possible reasons for this discrepancy during the latter stages of the event, including downstream synoptic and mesoscale forcing, frictional drag and thermal dissipation, variations in the coastal orography, and decay by vertical radiation of gravity wave energy, all of which are absent from the inviscid reduced-gravity model. For example, simple estimates suggest a one-day frictional decay timescale, comparable to the duration of a coastal-trapped event (Samelson and Rogerson 1996).

Aircraft transects through the 10–11 June 1994 coastal-trapped wind reversal (Ralph et al. 1998, their Fig. 23) show a southward thickening of the stable layer above the boundary layer at the leading edge of the wind reversal and weak southward thinning of the boundary layer itself. This baroclinic structure has some similarities to the linear two-layer reduced-gravity model fields during the initial and transition phases (Figs. 9 and 10). The 250-km region near the leading edge of the disturbance at $t = 10^5$ s, where this similarity is evident, is indicated by a horizontal line in Fig. 9. In the region of greatest southward increase in the upper interface height, the lower interface height decreases southward. This structure appears qualitatively consistent with the aircraft observations. This vertical phase offset occurs in the model because the gravest mode begins to propagate away from the forcing region, in advance of the second mode, as the forcing reaches its maximum and begins to decrease. This propagation causes a weak lifting of the boundary layer ahead of the leading edge of the relatively large lifting of the stable layer that is centered just to the south of the forcing maximum. Thus, the boundary layer thickens slightly toward the north at the locations where the rapid northward decrease of the stable layer thickness dominates the overall structure. The model results suggest that a weak northward decrease in boundary layer thickness might have been observed if the aircraft transects had been continued farther north.

In general, the model upper interface deformations are much greater than the lower-layer deformations during the initial and transition phases (Fig. 9). As Ralph et al. (1998) remark, single-layer shallow water models cannot represent the simultaneous thickening of the stable layer and thinning of the boundary layer. Although the upper interface deforms much more than the lower interface, the lower interface disturbance does reach 100 m during the transition phase of the model response. The observations suggest that the change in the marine boundary layer thickness during the 10–11 June 1994 event was less than this, although changes of up to 50 m likely would not have been well resolved by the measurements.

Profiler observations also suggest the presence of a depth-independent northward flow during the initial stages of the 10–11 June 1994 event (Ralph et al. 1998, their Fig. 4), consistent with the initial velocity response in the model (Fig. 10). However, the observed northward flow extended far above the coastal orography, to roughly 6 km, so the correspondence in the lower atmosphere may be fortuitous. In the present model, vertical shear begins to develop in the alongshore velocity field near $t = 10^5$ s. A strong northward flow is found in the lower layer, which propagates more rapidly northward than the upper interface deformation. In contrast, the aircraft observations appear to place the maximum northward flow at the leading edge in a thin stable layer that merges with the boundary layer inversion at the leading edge. This observed velocity structure is not reproduced by the model. If a linear frictional drag is included in the lower layer, as a simple model of the turbulent transfer of momentum from the atmospheric boundary layer into the sea surface, then the lower-layer velocity response during the transition phase is substantially weaker but the basic structure of the interface response is unchanged (Figs. 11, 12). In that the largest velocities then occur in the stable layer above the boundary layer, the model response resembles the aircraft observations more closely with surface friction than without surface friction.

It should be noted here that the aircraft transect through the leading edge of the disturbance (Ralph et al. 1998, their Fig. 22) was close to the San Francisco Bay region, where the height of the coastal orography decreases below 200 m. This change in coastal orography may also have affected the observed disturbance and is not represented in the model. For example, the dependence of the trapped modes on step amplitude (Fig. 3) suggests that the decreasing orographic height could lead to steepening of the leading edge of the disturbance.

6. Summary

The vertical structure of coastal-trapped disturbances in several idealized models of the lower atmosphere has

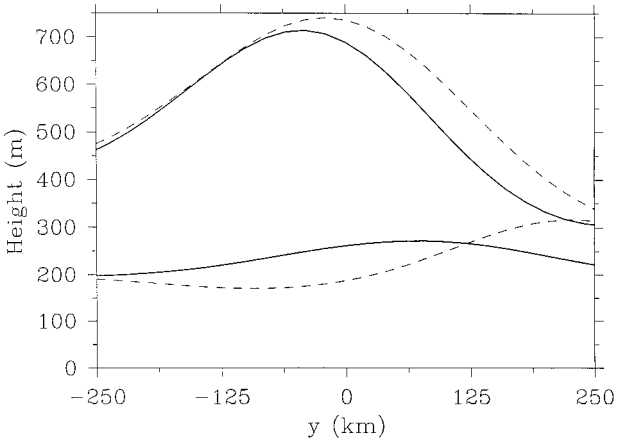

FIG. 11. Linear solutions of the two-layer numerical model with linear frictional drag in the horizontal momentum equations. The drag coefficient is $R = r/H$, where $r = 0.01$ m s^{-1} and $H = 200$ m. Interface heights at $x = 0$ are shown for -250 km $< y <$ 250 km for $t = 10^5$ s (thick line) and $t = 1.25 \times 10^5$ s (dashed line). The pressure forcing amplitude is $P_F = -1.5$ mb.

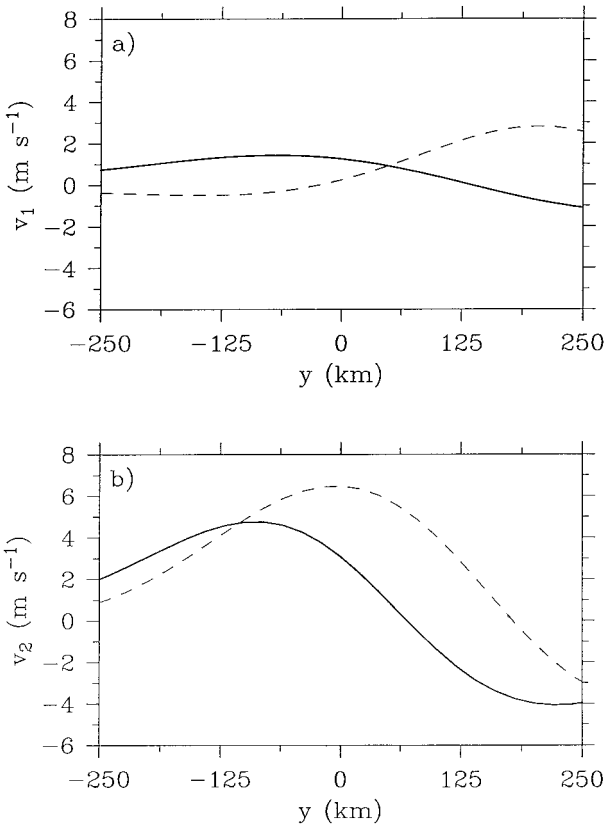

FIG. 12. As in Fig. 11 but for northward velocity in (a) layer 1 and (b) layer 2.

been examined. The presence of a stable layer above the boundary layer inversion increase the gravest mode phase speed and supports the existence of higher vertical modes. Results from a linear two-layer reduced-gravity model suggest that the observed vertical structure of isotherms at the leading edge of the 10–11 June 1994 event may arise during a transition from a directly forced, barotropic, alongshore velocity response to a regime influenced by wave propagation, as the coastal-trapped vertical modes excited by the mesoscale pressure gradients begin to disperse at their respective phase speeds (Figs. 9–12). The results suggest that the observed vertical structure of alongshore velocity, with largest velocities in the stable layer above the boundary layer, may arise from the effect of drag at the sea surface, which retards the flow in the boundary layer (Figs. 11, 12). The amplitudes of the linear model response and the observed isotherm displacements both suggest that nonlinear effects should be important, so the linear results must be interpreted with caution. Many other processes must also contribute to the observed structure. Nonetheless, it is interesting that a simple forced linear model does appear to reproduce some previously unexplained aspects of the vertical structure of the 10–11 June 1994 coastal-trapped disturbance.

Acknowledgments. This research was supported by the Office of Naval Research, Grant N00014-93-1-1369, code 322MM. I am grateful to J. Reisner and P. Smolarkiewicz for providing their numerical code, a modified version of which was used for the calculations in section 4, and to D. Durran for a careful reading of the manuscript.

APPENDIX A

Step-Trapped Modes

The eigenvalue problem (9)–(14) for trapped wave modes over step orography is solved following Chapman (1982). Separation of variables leads to the expansions

$$P^- = \sum_{n=0}^{\infty} A_n e^{\alpha_n \xi} \cos\mu_n \zeta, \quad P^+ = \sum_{n=0}^{\infty} B_n e^{-\beta_n \xi} \cos\nu_n (\zeta - h), \tag{A1}$$

where

$$\mu_n = \left(n + \frac{1}{2}\right)\pi, \qquad \nu_n = \left(n + \frac{1}{2}\right)\pi/d,$$
$$\alpha_n = (\mu_n^2 + \lambda^2)^{1/2}, \qquad \beta_n = (\nu_n^2 + \lambda^2)^{1/2}, \tag{A2}$$

and $d = d_s/H$. The pressure condition (13) on $h < \zeta < 1$ is applied by substituting the series expansions (A1), multiplying by $\cos\nu_m(\zeta - h)$, and integrating over ζ from h to 1. This yields

$$B_m = \frac{2}{d} \sum_{n=0}^{\infty} Q_{nm} A_n, \tag{A3}$$

where

$$Q_{mn} = \int_h^1 \cos\mu_m\zeta \cos\nu_n(\mathrm{s} - \mathrm{h})\, d\zeta. \qquad \text{(A4)}$$

The velocity condition (14) is applied similarly, with multiplication by $\cos\mu_m\zeta$ and integration over ζ from 0 to 1, which yields

$$(c'\alpha_m - 1)A_m = -2\sum_{n=0}^{\infty}(c'\beta_n - 1)B_nQ_{mn}. \qquad \text{(A5)}$$

Substitution of (A3) into (A5) and truncation of the series to a finite number of modes yields a standard generalized matrix eigenvalue problem with eigenvalue c',

$$c'(\boldsymbol{\alpha} + \frac{4}{d}\mathbf{Q}\boldsymbol{\beta}\mathbf{Q}^{\mathrm{T}})\mathbf{A} = \left(1 - \frac{4}{d}\mathbf{Q}\mathbf{Q}^{\mathrm{T}}\right)\mathbf{A}, \qquad \text{(A6)}$$

where $\mathbf{Q}$ and $\mathbf{A}$ are the matrix vector with elements Q_{mn} and A_n, $\mathbf{Q}^{\mathrm{T}}$ is the transpose of $\mathbf{Q}$, and $\boldsymbol{\alpha}$ and $\boldsymbol{\beta}$ are diagonal matrices with diagonal elements α_n and β_n. Eigenvalues and eigenvectors were obtained here using the MATLAB function eig, with truncation of the expansions (A1) at $n = N$ for $N = 50$ or $N = 100$, and analytic evaluation of the matrix elements Q_{mn}.

APPENDIX B

Two-Layer Internal Kelvin Waves

The Kelvin wave equations (25) and (26) are obtained as follows. Equations (20)–(22) are linearized around a step profile in potential temperature, $\theta = \theta_1$ for $0 < z < z_1$, $\theta = \theta_2$ for $z_1 < z < z_2$, and $\theta = \theta_3$ for $z > z_2$, and forced by an imposed pressure distribution $p_a(y, t)$ at the fixed height $z = H_a > z_2$. The linearized equations are

$$-fv_1 = -(a + b)\psi_{1x} - b\psi_{2x}, \qquad \text{(B1)}$$

$$-fv_2 = -b\psi_{1x} - b\psi_{2x}, \qquad \text{(B2)}$$

$$v_{1t} + fu_1 = -(a + b)\psi_{1y} - b\psi_{2y} + F_{ay}, \qquad \text{(B3)}$$

$$v_{2t} + fu_2 = -b\psi_{1y} - b\psi_{2y} + F_{ay}, \qquad \text{(B4)}$$

$$\psi_{1t} + \Psi_1(u_{1x} + v_{1y}) = 0, \qquad \text{(B5)}$$

$$\psi_{2t} + \Psi_2(u_{2x} + v_{2y}) = 0, \qquad \text{(B6)}$$

where the semigeostrophic approximation has also been made ($u_t \ll fv$) and the subscripts j, $j = 1, 2$, refer to quantities associated with the motion in layer j, which has potential temperature $\theta = \theta_j$. The constants a and b and the pressure forcing term F_{ay} are defined by

$$a = (\theta_2 - \theta_1)\Pi'(P_1), \qquad \text{(B7)}$$

$$b = (\theta_3 - \theta_2)\Pi'(P_2), \qquad \text{(B8)}$$

$$F_{ay} = -\theta_3\Pi'(P_a)p_{ay}, \qquad \text{(B9)}$$

where Ψ_j and P_j (and P_a) are the base-state values of ψ and p at the interface levels $z = z_j$ (and $z = z_a$), and prime denotes derivative with respect to the argument.

The solution may then be written in terms of the amplitudes $\psi^{\pm}$ in (23) and the wave equations (25) and (26). The lower-layer amplitudes $\psi_2^{\pm}$ in (24) and the constant $c_{\pm}$ and $d_{\pm}$ are defined by

$$\psi_2^{\pm} = \left(\frac{d_{\pm}c_{\pm}^2}{b\Psi_1} - 1\right)\psi_1^{\pm}, \qquad \text{(B10)}$$

$$d_{\pm} = 1 - \frac{a\Psi_1}{c_{\pm}^2}, \qquad \text{(B11)}$$

$$c_{\pm} = \left\{\frac{(a + b)\Psi_1 + b\Psi_2}{2} \pm \left[\left(\frac{(a + b)\Psi_1 + b\Psi_2}{2}\right)^2 - ab\Psi_1\Psi_2\right]^{1/2}\right\}^{1/2}. \qquad \text{(B12)}$$

With ψ_1 and ψ_2 known, the disturbance pressures p_1 and p_2 may be determined from

$$\theta_1\Pi'(P_0)p_0 = a\psi_1 + b(\psi_1 + \psi_2) + \theta_3\Pi'(P_a)p_a, \qquad \text{(B13)}$$

$$p_1 = p_0 - \psi_1, \qquad \text{(B14)}$$

$$p_2 = p_1 - \psi_2, \qquad \text{(B15)}$$

where P_0 and p_0 are the base-state and disturbance pressures at the surface ($z = 0$). The interface disturbances Z_1 and Z_2 may then be obtained from the hydrostatic relation, which yields

$$Z_1 = \frac{\theta_1}{g}(\Pi'(P_0)p_0 - \Pi'(P_1)p_1), \qquad \text{(B16)}$$

$$Z_2 = Z_1 + \frac{\theta_2}{g}(\Pi'(P_1)p_1 - \Pi'(P_2)p_2). \qquad \text{(B17)}$$

REFERENCES

Bannon, P. R., 1981: Synoptic-scale forcing of coastal lows: Forced double Kelvin waves in the atmosphere. *Quart. J. Roy. Meteor. Soc.;* **107,** 313–327.

Bond, N., C. Mass, and J. Overland, 1996: Coastally trapped wind reversals along the U.S. west coast during the warm season. Part I: Climatology and temporal evolution. *Mon. Wea. Rev.,* **124,** 430–445.

Chapman, D. C., 1982: On the failure of Laplace's tidal equations to model subinertial motions at a discontinuity in depth. *Dyn. Atmos. Oceans,* **7,** 1–16.

Dorman, C. E., 1985: Evidence of Kelvin waves in California's marine layer and related eddy generation. *Mon. Wea. Rev.,* **113,** 827–839.

——, 1987: Possible role of gravity currents in northern California's coastal summer wind reversals. *J. Geophys. Res.,* **92,** 1497–1506.

Gill, A. E., 1977: Coastally trapped waves in the atmosphere. *Quart. J. Roy. Meteor. Soc.*, **103,** 431–440.

——, 1982: *Atmosphere–Ocean Dynamics.* Academic Press, 662 pp.

Hermann, A. J., B. M. Hickey, C. F. Mass, and M. D. Albright, 1990: Orographically trapped coastal wind events in the Pacific North-

west and their oceanic response. *J. Geophys. Res.*, **95,** 13 169–13 193.

Holland, G., and L. Leslie, 1986: Ducted coastal ridging over S.E. Australia. *Quart. J. Roy. Meteor. Soc.*, **112,** 731–748.

Jury, M., C. MacArthur, and C. Reason, 1990: Observations of trapped waves in the atmosphere and ocean along the coast of southern Africa. *South Afr. Geogr. J.*, **72,** 33–46.

Mass, C. F., and M. D. Albright, 1987: Coastal southerlies and alongshore surges of the west coast of North America: Evidence of mesoscale topographically trapped response to synoptic forcing. *Mon. Wea. Rev.*, **115,** 1707–1738.

——, and N. Bond, 1996: Coastally trapped wind reversals along the United States west coast during the warm season. Part II: Synoptic evolution. *Mon. Wea. Rev.*, **124,** 446–461.

Nguyen, N. A., and A. E. Gill, 1981: Generation of coastal lows by synoptic-scale waves. *Quart. J. Roy. Meteor. Soc.*, **107,** 521–530.

Ralph, F. M., L. Armi, J. Bane, C. Dorman, W. Neff, P. J. Neiman, W. Nuss, and P. O. Persson, 1998: Observations and analysis of the 10–11 June 1994 coastally trapped disturbance. *Mon. Wea. Rev.*, **126,** 2435–2465.

Reason, C., and M. Jury, 1990: On the generation and propagation of the southern Africa coastal low. *Quart. J. Roy. Meteor. Soc.*, **116,** 1133–1151.

——, and D. Steyn, 1990: Coastally trapped disturbances in the lower atmosphere: Dynamic commonalities and geographic diversity. *Prog. Phys. Geogr.*, **14,** 178–198.

——, and ——, 1992: The dynamics of coastally trapped mesoscale ridges in the lower atmosphere. *J. Atmos. Sci.*, **49,** 1677–1692.

Rogerson, A. M., and R. M. Samelson, 1995: Synoptic forcing of coastal-trapped disturbances in the marine atmospheric boundary layer. *J. Atmos. Sci.*, **52,** 2025–2040.

Samelson, R. M., and A. M. Rogerson, 1996: Life-cycle of a linear coastal-trapped disturbance. *Mon. Wea. Rev.*, **124,** 1853–1863.

Thompson, W., T. Haack, J. Doyle, and S. Burk, 1997: A nonhydrostatic mesoscale simulation of the 10–11 June 1994 coastally trapped wind reversal. *Mon. Wea. Rev.*, **125,** 3211–3230.